OG 1032

BNL--42147

DE89 005770

SPIRAL SILICON DRIFT DETECTORS

P. Rehak
Brookhaven National Lab., Upton, NY 11973

E. Gatti, A. Longoni, M. Sampietro
Politecnico di Milano, 32 Piazza Leonardo da Vinci, 21033
Milano, Italy

P. Holl, G. Lutz
Max-Planck Institut für Physik und Astrophysik
Föhringer Ring 6, 8000 München 40, Western Germany

J. Kemmer, U. Prechtel and T. Ziemann
MBB ZTA12, Postfach 80 11 49, 8000 München 80, Western Germany

Paper presented at the 1988 IEEE Nuclear Science Symposium
Orlando, FL Nov. 9-11, 1988

SPIRAL SILICON DRIFT DETECTORS.

P. Rehak
Brookhaven Nat. Lab., Upton, NY 11973.

E. Gatti, A. Longoni, M. Sampietro
Politecnico di Milano, 32 Piazza Leonardo da Vinci, 20133 Milano, Italy*.

P. Holl, G. Lutz**
Max-Planck-Institut für Physik und Astrophysik
Föhringer Ring 6, 8000 München 40, Western Germany.

J. Kemmer, U. Prechtel and T. Ziemann
MBB ZTA12, Postfach 80 11 49, 8000 München 80, Western Germany.

ABSTRACT

An advanced large area silicon photodiode (and X-ray detector), called Spiral Drift Detector, was designed, produced and tested. The Spiral Detector belongs to the family of silicon drift detectors and is an improvement of the well known Cylindrical Drift Detector. In both detectors, signal electrons created in silicon by fast charged particles or photons are drifting toward a practically point-like collection anode. The capacitance of the anode is therefore kept at the minimum ($0.1pF$). The concentric rings of the cylindrical detector are replaced by a continuous spiral in the new detector. The spiral geometry detector design leads to a decrease of the detector leakage current. In the spiral detector all electrons generated at the silicon-silicon oxide interface are collected on a guard sink rather than contributing to the detector leakage current. The decrease of the leakage current reduces the parallel noise of the detector. This decrease of the leakage current and the very small capacitance of the detector anode with a capacitively matched preamplifier may improve the energy resolution of Spiral Drift Detectors operating at room temperature down to about 50 electrons rms. This resolution is in the range attainable at present only by cooled semiconductor detectors.

1. Introduction.

The Spiral Drift Detector belongs to the family of silicon drift detectors introduced by the authors several years ago[1]. The common feature of Silicon Drift Detectors is the transport of signal electrons parallel to the large detector surfaces toward a very small area anode. The direct consequence of this carrier transport is a very low anode capacitance (a typical value for large area cylindrical detectors is about $60fF$) and the independence of the capacitance on the detector size. A very small value of the detector capacitance decreases the series noise of the preamplifier and improves the total noise performance of the detector-readout system. The Silicon Drift Detectors achieved a remarkably good noise performance and position resolution [2].

Silicon Drift Detectors are realized on wafers where a large majority of the detector surface on both sides is covered by rectifying junctions. The junctions are held at different potentials to provide a drift field to transport signal electrons. The remaining surface areas between rectifying junctions are covered by thermally grown SiO_2. A thermally grown oxide layer always contains fixed positive charges. In equilibrium the positive charges in the oxide are compensated by mobile electrons in the silicon forming an accumulation layer at the $Si - SiO_2$ interface. When the detector bias voltages are applied, electrons are driven away from at least part of the interface accumulation layer. An interface depleted of accumulated electrons generates a relatively large amount of leakage current [3].

This paper presents a new design, called the Spiral Drift Detector, where electrons generated on the interface do not contribute to the detector leakage current. The spiral detector collects all electrons generated at the $Si - SiO_2$ interface on one or several guard sinks. The total leakage current collected on the detector anode is thus the sum of bulk generation and junction diffusion currents only.

There is one more problem connected with regions covered by oxide. Fixed positive charges within the oxide at the $Si - SiO_2$ interface modify the electric field in silicon close to the interface.

* This research is also supported by the Italian INFN and CNR.
** Also *MBB* GmbH

The resulting electric field has a tendency to move signal electrons created in silicon close to the interface toward the interface rather than into the bulk and toward the detector anode (see Fig. 1.1). We see that a narrow layer of silicon under the $Si - SiO_2$ interface is insensitive. This loss of a small part of the sensitive silicon volume (about 0.2%) has little importance for the charged particle or X-ray detections. For the detection of visible light, however, the sensitivity of the silicon surface is very important. The light is absorbed within a few microns and areas covered with oxide are practically light insensitive. The light sensitive side of the photodiode version of the detector should not have any area covered with oxide. Thus the light incident side of the detector, called p–side, has to be a continuous reverse biased rectifying junction held at a constant potential.

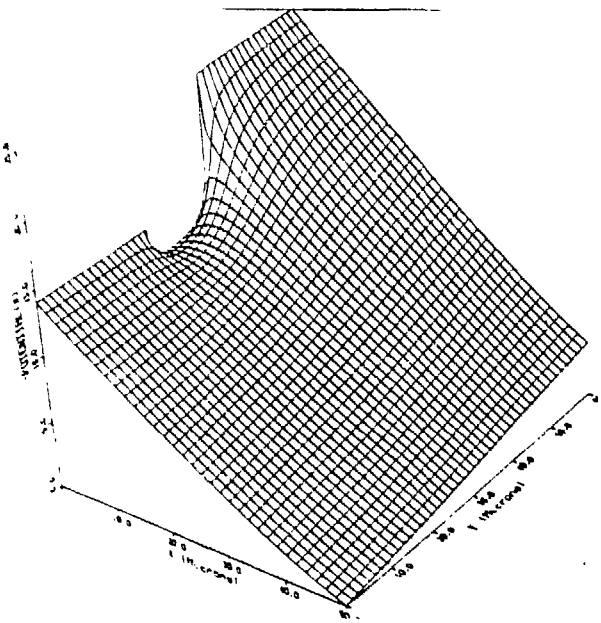

Fig. 1.1: Minus potential within the drift detector in a cross section close to the large detector surface. The x–coordinate measures the depth within the detector. $x = 0$ is the surface. The $Si - SiO_2$ interface is located between two rectifying junctions $23 \leq y \leq 37$ and at $x = 0$. Positive charges in the oxide bend the energy levels. Electrons generated at or very close to the surface are moving toward the interface.

The requirement of an equipotential on one side of the detector complicates the realization of the detector drift field. The "classical" drift detector of Ref. 1 has the same potentials applied from both sides of the wafer leading to a minimum potential energy for electrons in the middle of the wafer (Fig. 3 of Ref. 1). For a photosensitive application the potential can be varied on one side only (called n–side). Moreover, there are limits to the maximum voltage difference which can be applied along the n–side. The difference of potentials between p–side and any potential of p–implant at the n–side must be smaller than the depletion voltage across the thickness of the wafer to prevent large currents flowing in the reach-through condition. We see that the maximum voltage applied along the drift direction on the n–side is twice the depletion voltage.

There are many different ways to distribute this maximal drift voltage along the n–side. In Section 2 the optimum distribution of the potential on the n–side is derived. The transport of signal electrons within the bulk of the detector is studied and the distribution is obtained from the minimization of electron drift time.

Section 3 describes the design of the Spiral Drift Detector where all surface considerations are taken into account. Sink anodes are designed in a way to collect practically all leakage current generated at the $Si - SiO_2$ interface.

Section 4 presents some preliminary test results. Detectors were produced only recently and tests are still in progress.

2. Drift Field of Spiral Detector.

The "classical" drift detector of Ref. 1 has the same potentials applied on both sides of the wafer leading to a minimum potential energy for electrons in the middle of the wafer where electrons are transported (Fig. 3 of Ref. 1). The parabolic shape of the valley is due to the fixed positive charges of the ionized donors in the silicon bulk. The parabolic potential retains electrons in the middle of the detector. The transport of electrons toward the anode is due to a drift field which is superposed onto the retaining field. Both fields are to a high degree independent since the superposition of these two fields is a consequence of the linearity of the field equations. To realize the drift field in this straight forward way, potentials on both sides of the detector must change. The price to pay for an equipotential surface on the p–side of the detector is the loss of the independence of the drift field from the field due to the ionized donors.

Fig. 2.1 shows a realization of a drift field in the case where one side of the detector is held at a constant potential (suggested by F. Goulding from LBL). The computer simulation shows the negative potential within the detector about 3 mm from the anode. Changes of the potential along the n–side are sufficient to produce a drift field at the bottom of the valley. Electrons drift toward smaller values of y, that is, toward the center. At the same time the bottom of the valley moves closer to the n–side.

There are limits to how much one can vary the potential along the n–side of the detector. Without any loss of generality, let us define the anode potential as being 0 V. Close to the anode on the n–side, there is a p^+ structure roughly at the anode potential. The maximal negative potential Ψ on the p–side corresponds to the depletion voltage across the detector. The minimum of the potential energy of electrons (bottom of the valley) is located very close to the n–side. Any increase of the negative potential Ψ on the p–side would lead to a reach-through condition with a large current flowing between p^+ implants at both sides. Physically the reach-through condition means that the potential barrier for holes in the p^+ implant at the n–side has lowered and there are

many holes leaving the p^+ implant at the n-side and drifting towards the p-side.

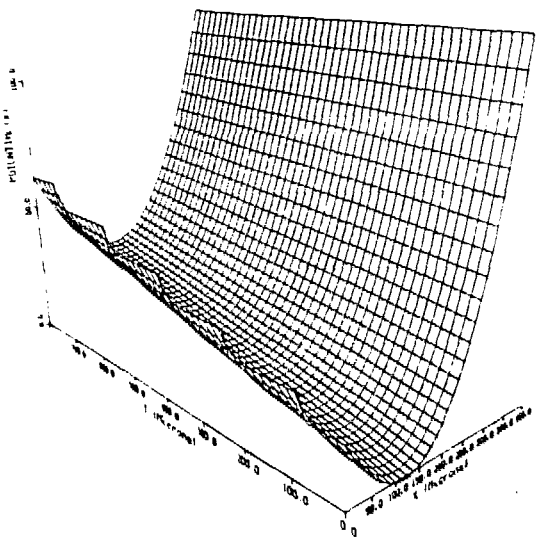

Fig. 2.1: Minus potential within the spiral detector in a cross section about 3 mm from the anode. The x-coordinate measure the depth within the detector. $x = 0$ is the n-side; $x = 400$ is the p-side. The y-coordinate is the radius minus 2.7 mm. There is a drift field toward smaller values of y. At the same time the bottom of the valley moves closer to the n-side where the anode is located.

The negative potential on the n-side of the wafer increases as we go farther away from the anode. At the same time the bottom of the channel moves away from the n-side as it can be seen in Fig. 2.1. At the outside radius of the detector the bottom of the valley is very near the p-side. Here again the voltage difference between p^+ implants on both sides of the detector cannot be larger than the depletion voltage of the detector. Otherwise a large reach-through current could flow as in the anode region, but in the opposite direction. The maximum negative voltage on the outside radius of the detector is twice the depletion voltage.

Beside the limitation we are left with the freedom to distribute the voltages in the radial direction along the n-side. The potential generated by the spiral structure on the n-side of the detector is such that the electron drift time is minimized. We are going to derive this optimum form of the drift field.

To simplify the problem, we assume that the potential changes much more rapidly across the wafer (x-direction) than along the radius of the detector (r-direction). Under this assumption Poisson's equation has to be solved in one dimension only (x-direction). The second dimension provides only the boundary conditions at both surfaces of the detector.

Poisson's Equation in x-coordinate:

$$\frac{d^2\phi_r(x)}{dx^2} = \frac{qN_D}{\epsilon_o \epsilon_{Si}} \tag{2.1}$$

where $\phi_r(x)$ is the negative potential at a general point (x, r) within the detector, q is the electronic charge, N_D is the volume donor density in the silicon bulk, ϵ_o is the permittivity and ϵ_{Si} is the relative dielectric constant of silicon. To save writing let as call ρ the combination of constants at right hand side of Eq. (2.1)

$$\rho = \frac{qN_D}{\epsilon_o \epsilon_{Si}}. \tag{2.2}$$

With our choice of zero potential at the anode and calling w the detector thickness the minus potential on the p side Ψ can be written:

$$\Psi = \frac{\rho w^2}{2}. \tag{2.3}$$

The solution of the 1-dimensional Poisson equation (2.1) is a parabola. The boundary conditions are the potentials on the two sides of the detector. For $x = 0$, that is, on the n-side $\phi_r(x = 0) = \Phi_r$ and for $x = w$, that is, on the p-side $\phi_r(x = w) = \Psi$. The solution of Eq. (2.1) with these boundary conditions is

$$\phi_r(x) = \frac{\rho x^2}{2} + \left(\frac{\Psi - \Phi_r}{w} - \frac{\rho w}{2}\right) x + \Phi_r. \tag{2.4}$$

Eq. (2.4) gives the negative potential at all points (x, r) of the detector as a function of the negative potential on the n-side Φ_r. The optimal form of Φ_r has to be found to minimize the drift time of electrons in the detector. In our 1-dimensional approximation electrons are transported at the minimum of $\phi_r(x)$ with respect to x for any value of r. The minimum of $\phi_r(x)$ can be found simply be equating to zero the derivative of $\phi_r(x)$ with respect to x. For a given r, the value of x_r minimizing $\phi_r(x)$ is

$$x_r = \frac{w}{2} + \frac{\Psi - \Phi_r}{\rho w} \tag{2.5}$$

and the corresponding potential is

$$\phi_r(\mathrm{min}) = \frac{\Psi + \Phi_r}{2} - \frac{\rho w^2}{8} - \frac{(\Phi_r - \Psi)^2}{\rho w^2} \tag{2.6}$$

The electron drift time from $r + \Delta r$ to r can now be calculated as the ratio of the traveled distance and the electron velocity. The velocity is given as the product of the mobility μ and the electric field E_D at the point x_r.

$$\Delta t = \frac{\Delta s}{\mu E_D} = \frac{\Delta s^2}{\mu\left(\phi_{r+\Delta r}(\mathrm{min}) - \phi_r(\mathrm{min})\right)} \tag{2.7a}$$

$$\Delta t = \frac{1 + (dx_r/dr)^2}{\mu\left(d\phi_r(\mathrm{min})/dr\right)} \Delta r \tag{2.7b}$$

Using Eqs. (2.5) and (2.6) we can substitute for the two derivatives in Eq. (2.7b) and express Δt as the function of Φ_r. The total drift time can then be written as the following integral

$$t = \frac{1}{\mu} \int_{r_{min}}^{r_{max}} \frac{(\rho w)^2 + (\Phi_r')^2}{\left[1/2\,(\rho w)^2 - \rho(\Phi_r - \Psi)\right] \times \Phi_r'} dr. \tag{2.8}$$

Eq. (2.8) is a classical functional given as an integral of a function F which depends on the unknown function Φ_r and its

derivative with respect to r ($\Phi'_r \equiv d\Phi_r/dr$). Moreover, the integrated function F does not depend explicitly on the independent variable r and we can write directly the first integral of the Euler equation:

$$\frac{\partial F}{\partial \Phi'}\Phi' - F = const \tag{2.9}$$

where

$$F = \frac{(\rho w)^2 + (\Phi'_r)^2}{\left[1/2\,(\rho w)^2 - \rho(\Phi_r - \Psi)\right] \times \Phi'_r}. \tag{2.10}$$

Following the prescriptions of Eq. (2.9) we obtain a simple first order differential equation for Φ_r.

$$\Phi'_r\left[1/2\rho w^2 - (\Phi_r - \Psi)\right] = c_1 \tag{2.11}$$

Eq. (2.11) is integrable. Two integration constants follow from conditions for Φ_r at $r = 0$ and $r = R$ (R is the outer radius of the detector) $\Phi_{r=0} = 0$; $\Phi_{r=R} = 2\Psi\,(= \rho w^2)$. After some manipulations we obtain a relatively simple result:

$$\Phi_r = \rho w^2\left(1 - \sqrt{1 - r/R}\right) \tag{2.12}$$

The form of Φ_r from Eq. (2.12) substituted into Eq. (2.5) gives us the position of the valley in the detector as a function of r.

$$z_r = w\left(1 - \sqrt{1 - r/R}\right) \tag{2.13}$$

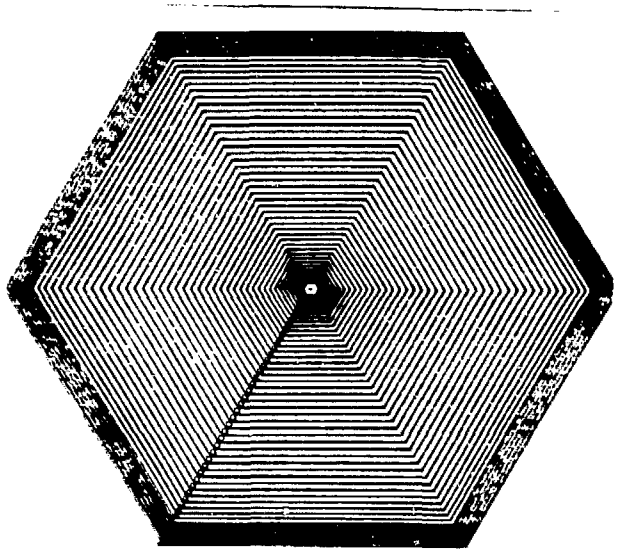

Fig. 2.2: n-side of the spiral detector. Two intertwined hexagonal spirals are visible. The wider spiral is a rectifying p^+ implant; the narrower spiral is the thermally grown SiO_2. Both spirals are running from the outer radius to the center of the detector where the signal anode is located.

Let us make two comments about the above solution of the variational problem. First, the radial drift velocity of electrons dr/dt in the optimized field is practically constant. We see the optimum solution leads to a linear relation between the radius and the drift time. This linearity may be used in applications where the radial position information is required.

Second, the derivative of Eq. (2.13) with respect to r has a singularity at $r = R$. The minimum of potential energy should be close to the p-side for $r \to R$, that is, close to the outside radius. The optimum solution of (2.13), however, requires that the valley should move away from the p-side with a diverging rate. It is impossible to realize such a field. Practically the behaviour of the Eq. (2.13) at $r = R$ means that we cannot use the full difference of voltages between two sides to realize the drift field.

The potential on the n-side of the designed detector is distributed very close to the function given by Eq. (2.12). The only deviations are at the outside radius and close to the anode region. Fig. 2.2 shows the n-side of the Spiral Drift Detector. (The n-side is the side with the electrode structure on it.) The opposite side (not shown) is a simple hexagon continuously implanted with Boron to create a shallow rectifying junction. The geometry shown in Fig. 2.2 is hexagonal instead of the normal circular geometry. The hexagonal spiral allows a complete covering of larger surfaces by placing several detectors into a two dimensional compact array. The radius of the detector is about 7 mm, the detector thickness is $400\mu m$.

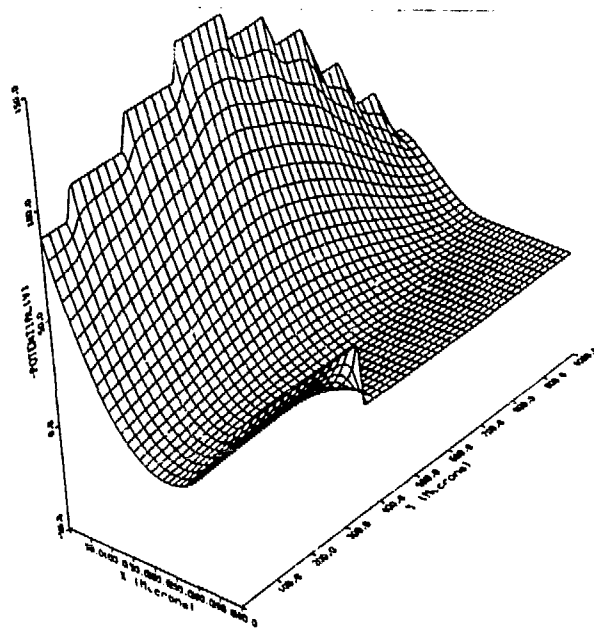

Fig. 2.3: Negative potential in the outside part of the detector. The zero value in the Figure is shifted and is -210 V. The x coordinate measures the depth within the detector. $x = 0$ is the n-side; $x = 400$ is the p-side. The y-coordinate is the radius minus 5.2 mm. We can see the division of the silicon volume into the external and the internal (sensitive) part.

There are two intertwined hexagonal spirals shown in Fig. 2.2. The resistance of the rectifying p^+ spiral forms a voltage divider. The spiral has a very small pitch as compared to the radius and

the geometry has almost a cylindrical symmetry which produces practically a radial drift field. The pitch and the width of the p^+ implanted spiral was changed in a way that a constant current in the spiral produces potential distribution given by Eq. (2.12).

The five largest spiral turns in Fig. 2.2 are guard turns. The highest negative voltage is applied at the first wide turn at the 7 o'clock position. The negative potential in the outer part of the spiral detector is shown in Fig. 2.3. We can see the division of the silicon volume into the external and the internal (sensitive) part. The external part is undepleted and held at -210 V. The internal part starts at $y = 300$ with a saddle point. The gradual decrease of the negative potential on the n-side is generated by turns of the spiral in the guard region. The end point of the guard part of the spiral is at the same potential as the p-side and about 30 V above the undepleted outside bulk.

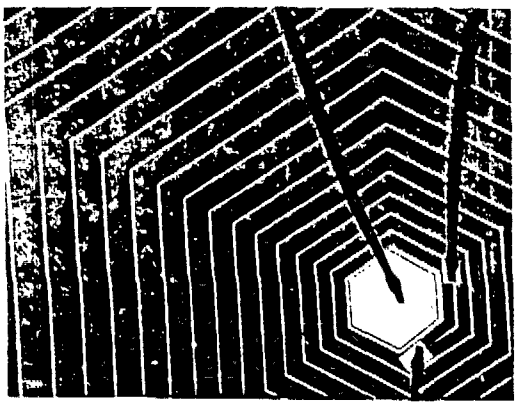

Fig. 2.4: Microphotograph of the central part of the detector. The large central hexagon is the anode. The lower bond is the connection to the final closed turn of the p^+ spiral. The bond at the right hand side is the connection to the guard sink.

The lowest negative drift voltage is applied at the central terminal of the spiral. Fig. 2.4 is a microphotograph of the central region of the detector. The p^+ spiral ends in a closed hexagon around the central anode. The potential at any point of the spiral is determined by the spiral geometry and produced by the current in the spiral. The resulting electric field in the detector transports signal electrons created anywhere within the sensitive volume of the detector toward the central anode.

3. Collection of the Surface Generated Currents.

The non implanted surface again has the geometry of a hexagonal spiral and is covered with a thermally grown SiO_2. There are fixed positive charges in the SiO_2 close to the interface. The presence of these charges bends the energy bands in such a way that electrons are being held close to the interface. (It is nothing more than the simple electrostatic attraction between mobile electrons within the silicon and fixed charges in the oxide.) Fig. 1.1 shows the negative potential within a radial section, cut at a 7 o'clock orientation as seen in Fig. 2.2. The section is perpendicular to the main surface of the detector and only $50\mu m$ of the total silicon thickness in the x direction is shown. The $Si - SiO_2$ interface is located between two adjacent turns of the p^+ spiral. Electrons generated at the interface are going to the region near the interface where their potential energy becomes minimal. If the geometry were perfectly symmetric around the central anode, the electrons would accumulate at the interface, change the shape of the field there and finally start to fall into the main valley of the detector. The Spiral Drift Detector breaks the unwanted symmetry.

To see the field really well we would need a four dimensional display of the potential as a function of three spatial directions. To understand the field and the motion of electrons without a 4 D display we have to envision the shape of the potential in a radial section displaced by a small angle from the 7 o'clock orientation say at the 6 o'clock orientation in Fig. 2.2.

The negative potential looks similar to the one shown in Fig. 1.1, however, the absolute potential of the whole section is slightly shifted. The interface at the 6 o'clock cut is at a different potential than the potential of the interface at the 7 o'clock section because of the potential drop along the spiraling rectifying junction. Electrons generated at the interface move from the 7 o'clock position into the 6 o'clock position following the lower potential energy. The potential at the 5 o'clock position looks again similar to the potential at the 6 o'clock position, but the absolute values are different due to the potential drop of the current flowing along the p^+ spiral. Thus the electrons at the interface move also from the 6 o'clock position toward the 5 o'clock position.

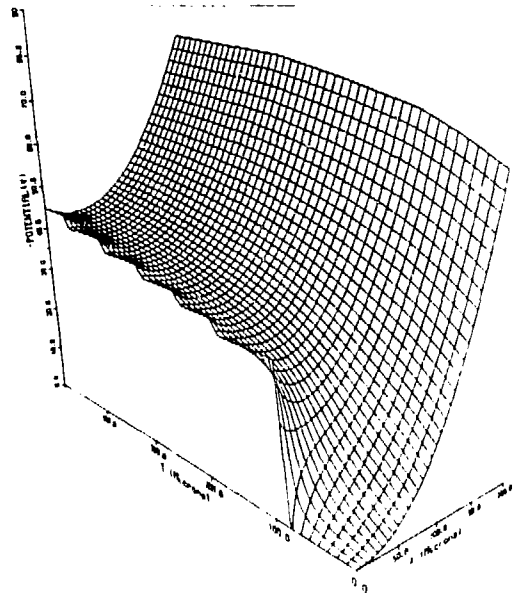

Fig. 3.1: Negative potential in a radial cross section close to the center of the detector. The main valley of the detector is visible. The anode is located at $y \leq 80\mu m$. Fine details of the potential close to $Si - SiO_2$ interface are not shown.

We can see that electrons generated at the interface move around and toward the center of the detector following the spiral geometry. At the central region, shown in Fig. 2.4, they reach the guard sink and are collected by an external circuit.

The negative potential in the central region is shown in Fig. 3.1. The detector anode is at a zero potential and the surrounding end of the p^+ spiral is biased at $-30V$. This large potential difference is needed to position the main potential valley of the detector sufficiently far from the surface. The guard sink, made by an n^+ implant is biased at -27 V.

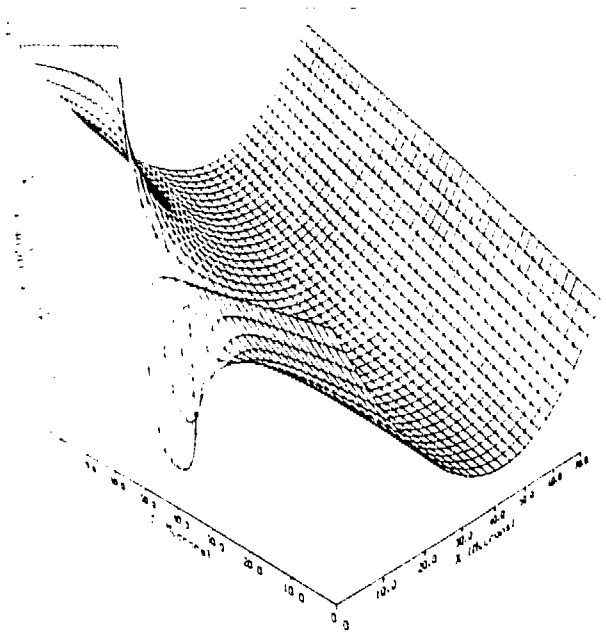

Fig. 3.2: Negative potential in the region of guard sink. The potential of the sink is at -27 V relative to the anode potential.

The detail of the potential at the guard sink is shown in Fig. 3.2. Electrons generated at the surface are collected here in spite of the fact that the potential of the anode is $27V$ higher that the potential of the sink. The saddle point located a few μm from the interface prevents electrons from the surface to reach the main valley of the detector and also prevents signal electrons to be collected by the guard sink. We see that the detector is effectively divided into the central signal region and the insensitive surface region.

4. Test Results.

Spiral Drift Detectors were fabricated at MBB using the planar technology[4]. Six closely related kinds of prototypes were produced all on $300\mu m$ thick silicon rather than on $400\mu m$ as planned.

All DC test, that is, I-V and C-V characteristics confirmed the basic physics of the design. The smaller thickness of the detectors as compared with the projected value leads to smaller values of bias voltages applied to the detector. Detectors were functioning properly under the following bias voltages. $U_{p-side} = -110V$, $U_{outer\ spiral} = -160V$, $U_{inner\ spiral} = -22V$, $U_{guard\ sink} = -18.5V$ and $U_{bulk} = -85V$. The detector leakage current at room temperature was about $1nA$; the anode capacitance was $0.1pF$.

We did not have a capacitively matched preamplifier during the test. The presented results were obtained with a commercially available RL-791/1 preamplifier[5], having a 2N 4416 JFET as an input transistor. The transistor capacitance was about $4pF$, the capacitance of the connection $3pF$ resulting in a total input capacitance of about $7pF$.

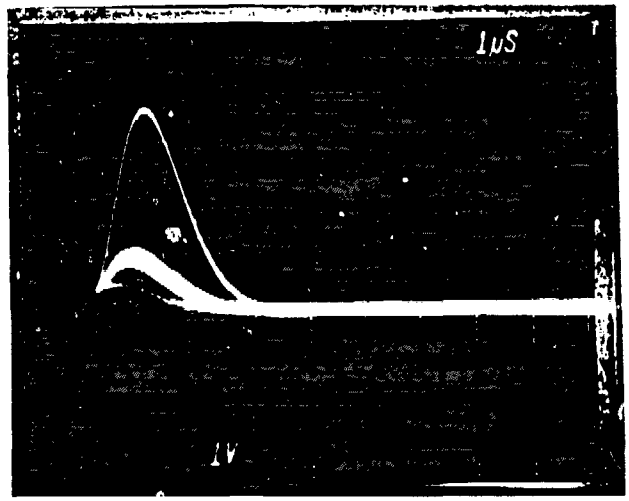

Fig. 4.1: Output waveform of the ORTEC-450 pseudo gaussian shaper ($\tau_{int} = \tau_{diff} = 0.5\mu s$). Detector was illuminated with an Am^{241} X-ray source.

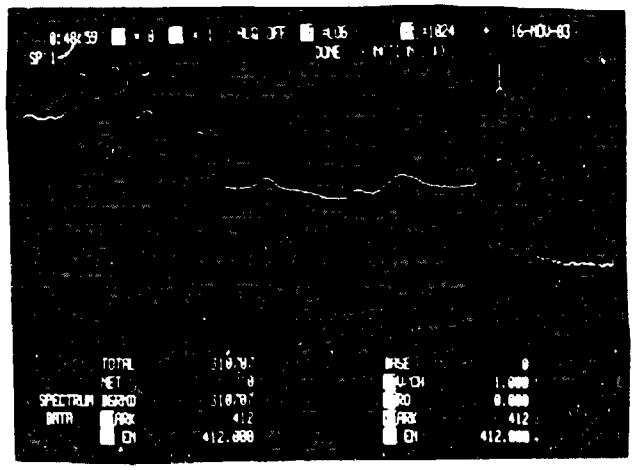

Fig. 4.2: Am^{241} X-ray spectrum obtained with a Silicon Spiral Detector and a commercially available preamplifier RL-791/1 (log scale).

The Am^{241} X-ray spectrum in Fig. 4.2 is displayed in a log scale and in Fig. 4.3 in a linear scale. The resolution is limited by the electronic noise which is 190 electrons. This noise is close to the calculated value for the 4416 FET, $7pf$ input capacitance and the pulse shape shown in Fig. 4.1. There is no indication of electron trapping down to a 1% level. Detectors are presently under an extensive test and more results will be published shortly.

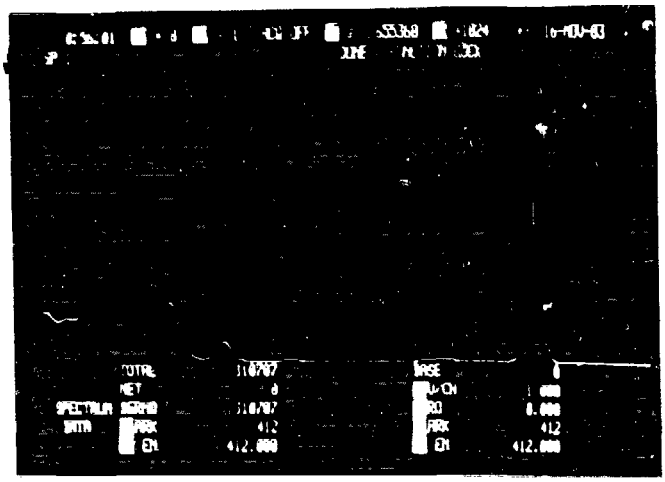

Fig. 4.3: Am^{241} X-ray spectrum obtained with a Silicon Spiral Detector and a commercially available preamplifier RL-791/1 (linear scale).

5. Conclusions.

An advanced large area silicon photodiode and X-ray detector was designed, produced and tested. The detector has a very small capacitance of about $0.1pF$ and a leakage current under $1nA$ at room temperature. With the commercial electronics the noise of the system is 190 electrons. The expected resolution with a capacitively matched electronics is about 50 electrons rms.

6. Acknoledgements.

We wish to thank V. Radeka for many stimulating discussions and, in particular, for the kind hospitality given to E. Gatti. We are indebted to P. Valier from *MBB* GmbH for the very fast and precise mounting of the drift detectors.

7. References

1. E. Gatti and P. Rehak, Nucl. Instr. and Meth. 225, 608 (1984).
2. P. Rehak et al., Nucl. Instr. and Meth. 248, 367 (1986).
3. A.S. Grove, *Physics and Technology of Semiconductor Devices*, J. Wiley and Sons, Inc., New York, 1967, Page 298.
4. J. Kemmer, Nucl. Instr. and Meth. 226, 89 (1984).
5. Produced by REL-LABS Inc., 30 Midland Avenue, Hickville, NY 11801.